Int J Clin Exp Pathol 2017;10(5):5406-5417
www.ijcep.com /ISSN:1936-2625/IJCEP0047985

Original Article

Detection of common chromosomal translocations and immunohistochemical analysis of soft tissue small round cell sarcomas

Yan Qi[1*], Jinli Zhang[2*], Hong Zou[1], Yan Ren[1], Ning Wang[1], Jin Zhao[1], Jianming Hu[1], Jinfang Jiang[1], Wei Jia[1], Lijuan Pang[1], Feng Li[1,3]

Departments of [1]Pathology and The Laboratory of Xinjiang Endemic and Ethnic Diseases, [2]Biochemistry and Molecular Biology, School of Medicine, Shihezi University, Shihezi, Xinjiang, China; [3]Department of Pathology, Beijing Chaoyang Hospital, Capital Medical University, Beijing, China. [*]Equal contributors.

Received May 19, 2015; Accepted March 30, 2017; Epub May 1, 2017; Published May 15, 2017

Abstract: Soft tissue small round cell sarcomas (SRCSs) are difficult to diagnose accurately by light microscopy. In this study, we analyzed the clinicopathological and genetic features of soft tissue SRCSs to help clinicians and pathologists better understand this entity. We clinicopathologically analyzed soft tissue SRCSs obtained from seven alveolar rhabdomyosarcoma (ARMS), seven primitive neuroectodermal tumor (PNET), four poorly differentiated synovial sarcoma (PDSS), and two round cell myxoid liposarcoma (RCMLS) patients, and developed a multiplex (m) RT-PCR assay to diagnose these sarcoma types using a subset of type-specific genes. The examined tumor types predominantly occurred in male children or adolescents, largely within the limbs. Tumors ranged in size from 1-10.5 cm (median, 5.0 cm), were typically not encapsulated, and exhibited infiltration of surrounding muscle and adipose tissue. Histological analysis detected small, round, blue cells with generally less cytoplasm and obviously nuclear atypia; some cases presented mucous, hyalinization, or a Ewing-PNET structure. Long-term follow-up revealed recurrences or metastases, and the prognosis of all patients, except for RCMLS patients, was very poor. Indeed, immunohistochemical and mRT-PCR analyses using a panel of monoclonal antibodies and primers specific for these fusion genes, respectively, enabled successful diagnosis of all 20 individuals. Taken together, our mRT-PCR method can be used to examine the expression levels of multiple genes within a single reaction, as each fusion gene is specific to soft tissue SRCSs. The results of this study could be useful for rapid confirmation of SRCS diagnoses.

Keywords: Soft tissue small round cell sarcomas, fusion gene, multiplex RT-PCR, pathological diagnosis

Introduction

Sarcomas are a heterogeneous group of tumors, and small round cell sarcomas (SRCSs) represent a special group of highly aggressive malignant neoplasms, which, are morphologically characterized as predominantly small and monotonous undifferentiated cells with high nucleocytoplasmic ratios on histology [1]. In addition to morphological and immunohistochemical (IHC) profiling, advanced molecular biology techniques are required for an accurate diagnosis of these sarcomas; however, for some SRCSs, the cellular origin remains unclear. Molecular analyses are also very useful for the differential diagnosis of SRCSs. Recently, Taylor et al. [2] reported that sarcomas can be broadly classified into two categories, each containing clinically diverse sarcomas. The first category includes sarcomas caused by simple genetic alterations, including translocations or specific activating mutations. The second category includes tumors with complex and unbalanced karyotypes. SRCSs belong to the former category, with most being caused by a specific translocation event, including Ewing's sarcoma/primitive neuroectodermal tumor (ES/PNET) or extraskeletal Ewing's sarcoma, alveolar rhabdomyosarcoma (ARMS), desmoplastic small round cell tumor, and poorly differentiated synovial sarcoma (PDSS). These SRCSs are often indistinguishable by microscopy or immunophenotyping, making their diagnosis problematic in certain intractable cases.

In particular, accurate diagnosis of soft tissue SRCSs by light microscopy is extremely difficult. In the past decade, however, advances in polymerase chain reaction (PCR) technology and other DNA signal and target amplification techniques have resulted in the popular use of molecular diagnostics for soft tissue tumors [3-5].

Thus, traditional diagnostic approaches have recently come to be supplemented with several reliable molecular diagnostic tools to detect tumor type-specific genetic alterations. In addition, the successful application of some of these techniques to formalin-fixed paraffin-embedded (FFPE) tissues has made it possible to subject a broader range of clinical materials to molecular analysis. Molecular genetics has already become an integral part of the work-up of small, blue, round cell tumors that demonstrate characteristic translocations [6]. In multiplex reverse transcription PCR (mRT-PCR), more than one target sequence can be amplified simultaneously by including more than one pair of primers in the reaction. Therefore, mRT-PCR has the potential to offer considerable savings in both time and effort within the laboratory, without compromising testing efficacy or applicability [7]. Currently, the application of mRT-PCR is less common for SRCSs than others tumor types. Following the first description of its use in SRCSs by James et al. [3], Peter et al. [8] used this technique to diagnose 79 cases of soft tissue sarcoma, and indicated that the development of this method constitutes an important step toward the complete automation of detection of cancer-specific gene fusions. Here, we review SRCS cases to provide a theoretical and practical basis for the development and optimization of mRT-PCR systems, and discuss the application and potential of this technique to the field of soft tissue SRCS diagnostics.

Materials and methods

Tissues

In this study, we evaluated consecutive soft tissue SRCSs that were collected from consultation case files at the Department of Pathology, Shihezi University, School of Medicine, China. All cases were carefully reviewed, and diagnoses were made according to the 2001 World Health Organization classification criteria. Hematoxylin and eosin-stained sections (4-μm thick) from each patient were re-examined. In total, 20 SRCS tissues with monotonous undifferentiated cells and high nucleocytoplasmic ratios were included in the study, including tissues from seven ARMS, seven PNET, four PDSS, and two round cell myxoid liposarcoma (RCMLS) patients. This study was approved by the internal review board of the Shihezi University School of Medicine.

IHC staining

FFPE tissue sections were subjected to IHC staining after steam heat-induced epitope retrieval or pepsin digestion using a Dako Envision detection system (Dako, Glostrup, Denmark), according to the malk anufacturer's instructions. Sections were stained with the following primary antibodies (all purchased from Dako): monoclonal antibodies specific to vimentin (1:100), desmin (1:100), sarcomeric actin (1:50), MyoD1 (1:50), myogenin (1:25), cytokeratin (CK: AE1/AE3; 1:100), neuron-specific enolase (NSE) (1:100), CgA (1:100), CD99 (1:200), and S-100 (1:100); and polyclonal antibodies specific to myoglobin and alpha-smooth muscle actin (1:100 each). Specific immunostaining was verified by reference to previously confirmed positive and negative control tissue sections. IHC staining of FLI1 was conducted using a specific polyclonal antibody (1:600) (Santa Cruz Biotechnology, Dallas, TX, USA), according to the method described by Folpe et al. [9], but with minor modifications.

RNA extraction

Extraction of RNA from paraffin-embedded tumor samples was performed as described previously [10]. In brief, 15 5-μm thick sections were prepared from each representative paraffin-embedded tumor sample and collected in 2.0-mL sterile microtubes. After deparaffinization, the pellets were minced in 250 μL of lysis buffer [20 mmol/L Tris-HCl (pH 8.10), 20 mmol/L ethylenediaminetetraacetic acid, and 2% sodium dodecyl sulfate] and then mixed with 10 μL proteinase K (20 mg/mL, Merck, Germany). After incubation at 55°C overnight, 1 mL of Trizol reagent (Gibco BRL, USA) was added to each sample, and total RNA was extracted according to the manufacturer's instructions. The resulting RNA pellets were resuspended in 10-40 μL diethylpyrocarbonate-treated water.

Table 1. Oligonucleotide primers used for multiplex RT-PCR amplification of SRCSs

Primers	Sequnece	Product size (bp)	Annealing temperature (Tm°C)
EWS-281-F	5'TCCTACAGCCAAGCTCCAAGTC3'	155-270	59
EWS-281-R	5'ACTCCCCGTTGGTCCCCTCC3'		59
22.3N EWS (N)	5'CCAACAGAGCAGCAGCTACG3'	155-270	63
11.3n FLI1 (N)	5'GGTGATACAGCTGGCGTTGG3'		63
PAX3	5'CCAACCCCATgAACCCCACC3'	185	57 (60*)
FKHR-A	5'CTCTGGATTGAGCATCCACC3'		57
FKHR-B (S-N)	5'TCCAGTTCCTTCATTCTGCA3'	147	60
SYT-403-F	5'CCAGGGCAGCAAGGTTAC3'	203	57 (59*)
SYT-M-F (S-N)	5'CAGGGCTACGGTCCTTCAC3'		57
SSX-M-R	5'TTCGTCCTCTGCTGGCTTC3'	174	59
TLS	5'-CAGAGCTCCCAATCGTCTTACGG-3'	220	
CHOP	5'-GAGAAAGGCAATGACTCAGCTGCC-3		57
β-actin-F	5'GAGCGGGAAATCGTCCGTGACATT3'	234	55
β-actin-R	5'GATGGAGTTGAAGGTAGTTTCGTG3'		55

(N): nested primer, (S-N): semi-nested primer, *nested or semi-nested annealing temperature.

mRT-PCR

Principle of mRT-PCR: While a number of review and research articles have provided detailed descriptions of the key parameters that may influence the performance of standard PCR [11], fewer publications have discussed the factors influencing multiplex PCR [12, 13].

The sequences, specificity, and sensitivity of the oligonucleotide primers used in this study for detecting fusion genes in SRCS tissues were designed and determined using Oligo6.0 and PrimerPremier6.0 software. **Table 1** provides a summary of the primer characteristics. All oligonucleotide primers were tested for primer-dimer formation using Pubmed NCBI Blast software. In designing the mRT-PCR primers, the following steps/rules were tested and proven to be useful:

1) Length of individual primers between 18 and 24 bases. 2) It is desirable (but not absolutely necessary) that the two primers have similar melting temperatures (within ~5°C). 3) A purine: pyrimidine content of roughly 1:1 (40-60%). 4) If possible, the primer sequence should start and end with 1-2 GC pairs. 5) Non-complementation during primer design. 6) Primers generate products less than 400 base pairs in length.

Using these rules, multiplex PCR products differing from each other by 30-40 bp in length could be conveniently separated in commonly used 2% agarose gels.

Multiplex nested RT-PCR amplification: Nested multiplex RT-PCR was used to detect the PAX3-FKHR, EWS-FLI1, SYT-SSX, and TLS-CHOP fusion genes in ARMS, ES/PNET, PDSS, and MLS/RCL tissues, respectively. The optimal conditions for the multiplex assay were determined after several trials (data not shown). Initially equimolar concentrations of each primer were used; however, it was necessary to empirically change the proportions of various primers to obtain the best amplification results. Reaction mixtures for RT-PCR comprised 2 μL of extracted nucleic acids, 5 μL 10× PCR buffer, 1 μL dNTPs (25 mM, 200_M), 25 pmol upstream and downstream primers (**Table 1**), 1 μL enzyme mixture, and 0.1 μL Rnase inhibitor (40 U/μL). Mixtures were then incubated at 50°C for 30 min for reverse transcription of cDNA, followed by 95°C at 15 min to inactivate the reverse transcriptase. Amplification was then carried out as follows: 40 cycles of denaturation for 30 s at 94°C, annealing for 45 s at 57°C, and elongation for 1 min at 72°C. Although all viral genomes can be amplified specifically at different annealing temperatures by monoplex PCR, our experience showed that lowering the annealing temperature to 57°C in the first round of RT-PCR was required for coamplification of fusion genes in the multiplex reaction. For nested PCR amplification, 1 μL of the amplified DNA from the first round of PCR was used in a new 25-μL reaction containing 25 pmol of each inner primer [22.3N EWS (N)/11.3n FLI1(N) for EWS-FLI1, PAX3/FKHR-B(S-N) for PAX3-FKHR, TLS/CHOP for TLS-CHOP, and SYT-403-F/SSX-M-R(S-N) for SYT-SSX]. After 5 min heating at 95°C, reactions were incubated at 94°C for 1 min, 53°C for 1 min, and 72°C for 1 min for 30 cycles. Thermal cycling was carried out in a programmable heat block (Gene Amp PCR System 2400; Applied Biosystems, Foster City, CA, USA). The results were analyzed by 2% agarose gel electrophoresis with ethidium bromide staining. Standard

Table 2. Clinical features in 20 cases of soft tissue small round cell sarcomas

No.	Age (yr)/sex (M/F)	Location	Size (cm)	Current diagnosis	Metastases	Status at last follow-up
C1	15/M	Retroperitoneum	4	PNET	NA	DOD
C2	16/F	Left hip	12	PNET	NA	DOD
C3	28/M	Left ethmoid sinus	3.5	PNET	Lung	DOD
C4	36/F	Dorsum of right foot	2.5	PNET	NA	DOD
C5	35/M	Right upper extremity	9	ARMS	Lung	DOD
C6	7 month/M	Left nose	2.2	ARMS	NA	DOD
C7	25/M	Right elbow	5	ARMS	NA	NA
C8	1/M	Left neck	2.3	ARMS	Lung	DOD
C9	11/F	Right cheeks	4	ARMS	NA	DOD
C10	30/M	Right upper extremity	1	ARMS	NA	NA
C11	11/F	Thoracic wall	3.5-6	PNET	NA	DOD
C12	23/M	Right jaw	3.4	ARMS	NA	DOD
C13	66/M	Left leg	7.4	RCMLS	Recurrence	RMAS
C14	41/F	Spinal canal	4.9	RCMLS	Lung retroperitoneal	AWD
C15	41/F	Lung	1.5	PNET	NA	AWD
C16	15/M	Left leg	10.5	cEMC/PNET	Lung	DOD
C17	19/M	Left leg ankle	8.5	PNET/PDSS	NA	DOD
C18	13/M	Left elbow	3	PDSS	Bone	DOD
C19	17/M	Left elbow	13	PDSS	NA	DOD
C20	40/F	Left thigh	7.5	PDSS	NA	NA

ARMS, Alveolar Rhabdomyosarcoma; PNET, Peripheral Neuroectodermal Tumors; RCMLS, Round Cell Myxoid Liposarcoma; Cellular extraskeletal myxoid chondrosarcoma cEMC; PDSS, Poorly Differentiated synovial sarcoma; F, female; M, male; NA, not available; DOD, died of disease; RMAS, Recurrence and metastasis after surgery; AWD, alive with disease; NA, not available.

precautions were applied in all the manipulations to reduce the probability of sample contamination. Separate areas were used for reagents, treatment of samples, and manipulation of amplified samples. Undiluted samples and 10-fold dilutions of nucleic acid extracts were analyzed twice in independent experiments to avoid false-negative results caused by inhibitors, as in certain cases diluted samples gave stronger positive signals than undiluted samples. A negative control was added for every two samples, and a positive control was added for each reaction. Nested PCR amplification products were sequenced at Shanghai Genecore Biotechnologies (Shanghai, China), and the resulting sequences were compared with those contained in the GeneBank database using the NCBI BLAST program.

Results

Clinical findings

Clinical data are summarized in **Table 2**. The patients were predominantly male [13 (65%) versus 7 (35%)], with the age of diagnosis ranging from 7 months to 66 years (mean, 22.8 years). The tumors arose with a wide anatomical distribution; however, most arose in the upper and lower limbs (10, 50%), followed by the head and neck region (5, 25%). The other tumors (5%) arose in the retroperitoneum, hip, spinal canal, lung, and thoracic wall, respectively.

Follow-up

Clinical follow-ups were available for 17 cases (seven ARMS, seven PNET, three PDSS, and two RCMLS cases), with the age of these patients ranging from 8 months to 7 years. At the time of the last follow-up, 14 patients had died, usually due to uncontrolled local disease (six cases of PNET, five cases of ARMS, and three cases of PDSS). These deaths occurred 1-20 years after the first diagnosis (mean, 5 years). The prognosis of all patients, except for RCMLS patients, was very poor (up to 4 recurrences, with a mean of 1.7). See **Table 2** for details.

Histopathological features

Tumor sizes ranged from 10 mm to 105 mm (mean, 50 mm). Grossly, the most common presentation of SRCS was the formation of a poor-

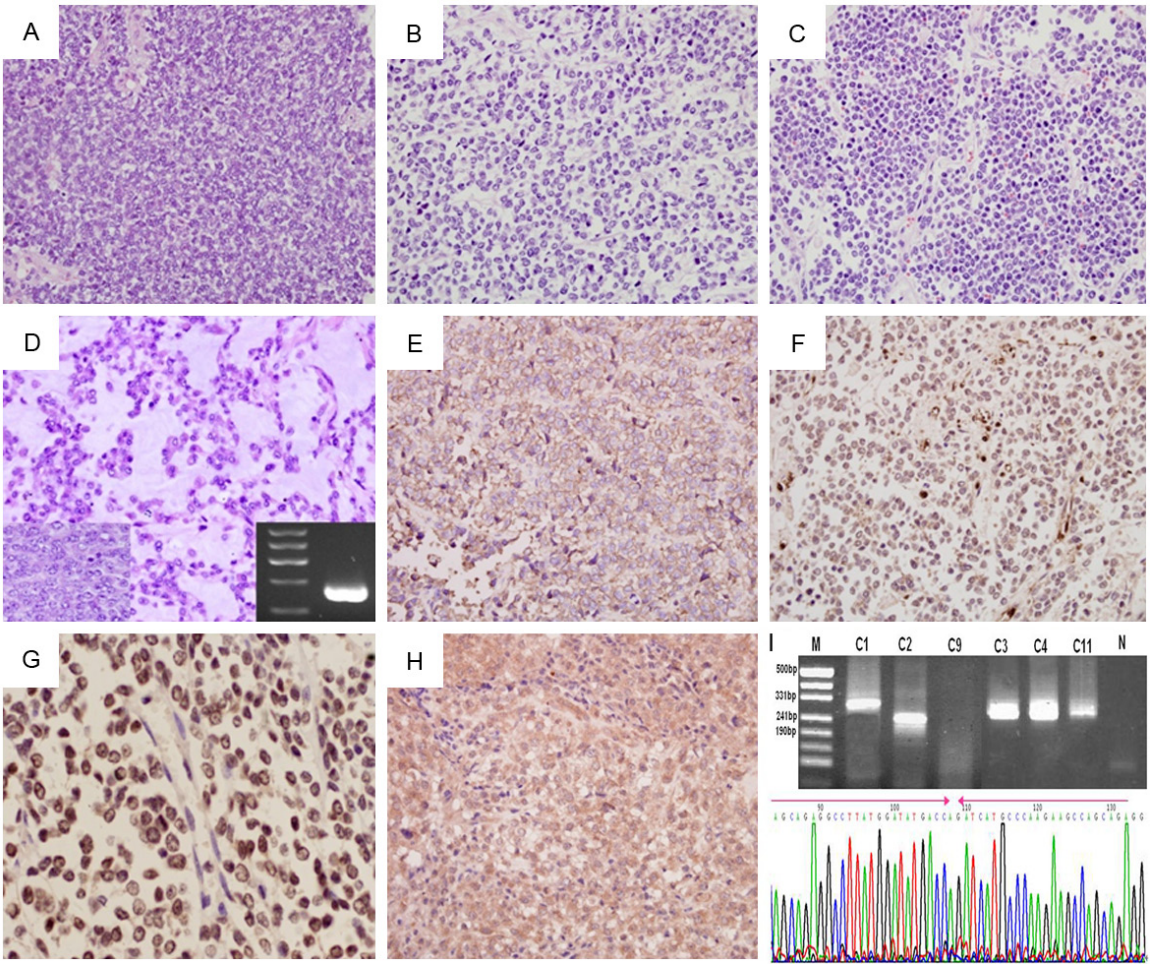

Figure 1. Histological, immunohistochemical, and reverse transcriptase-polymerase chain reaction (RT-PCR) analyses of Ewing's sarcoma/primitive neuroectodermal tumor (ES/PNET) tissues. A. Image showing diffuse distribution of small tumor cells from Patient 3; the shape and size of the tumor cells were relatively consistent. The tumor was initially diagnosed as lymphoma. B. Tumor cells in the interstitial tissues were divided by the alveolar structure and fibrous tissue (image of tissue from Patient 1). C. Image highlighting the presence of mononuclear cell-like lymphocytes in tissue from Patient 2. D. Patient 16 exhibited mucous components and tumor cells with abundant, eosinophilic cytoplasm. Portions of the tumor were comprised of small blue cells. E. Image of tissue from Patient 1 showing positive immunostaining for CD99 within the cytoplasm. F. Image of tissue from Patient 3 showing positive immunostaining for S-100 within nuclei. G. Images of tissues from Patients 1, 2, 3, 4, 11 showing positive immunostaining for Fli-1 shows within nuclei. H. Images of tissues that were positive for Desmin staining. I. Tissues from Patients 1, 2, 3, 4, and 11 were positive for the EWS-FLI-1 fusion transcript (155-270 bp), as determined by RT-PCR and confirmed by automated sequencing of the RT-PCR products.

ly defined soft tissue mass at any location, which is usually not encapsulated and infiltrates the surrounding muscle and adipose tissue. Each of the 20 cases showed the following features: 1) poor differentiation of the major tumor cells, presenting a solid pattern; 2) atypical morphology; 3) 2-3 mitotic figures per 10 high-power fields; 4) necrosis and hemorrhaging to some extent.

Histopathological examination of the seven PNET biopsy specimens detected small, round, or oval tumor cells and uniform cells with darkly stained nuclei and, in some cases, very scanty cytoplasm. Small tumor cells were diffusely distributed (**Figure 1A**), and the shape and size of the tumor cells were consistent (**Figure 2B**), with some cases showing areas of mononuclear cell-like lymphocytes or short spindle cells. Fibrous tissue split the tumor cells in the interstitial space (**Figure 1C**, **1D**). The seven ARMS specimens exhibited small tumor cells that were diffusely distributed, and the shape and size of the tumor cells were consistent, with

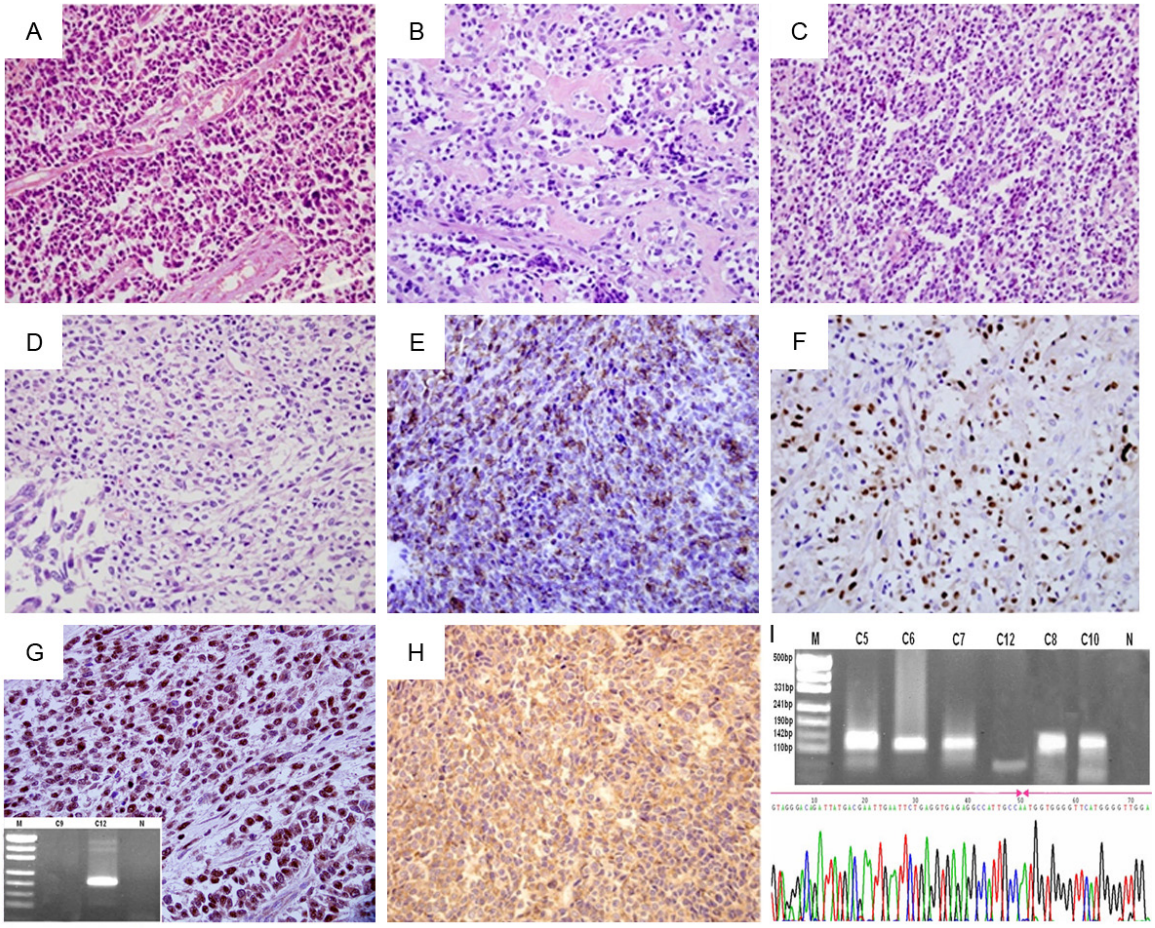

Figure 2. Histological, immunohistochemical, and reverse transcriptase-polymerase chain reaction (RT-PCR) analyses of alveolar rhabdomyosarcoma (ARMS) tissues. A. Image showing diffuse distribution of small tumor cells from Patient 5; the shape and size of the tumor cells were relatively consistent, and parts of the tumor exhibited cells with eosinophilic cytoplasm. B. Tumor cells in the interstitial tissues were divided by the alveolar structure and fibrous tissue (image is of tissue from Patient 6). C. Image of tumor cells from Patient 7, which appeared similar to monocytoid lymphocytes and were devoid of cytoplasm. D. Patient 9 exhibited tumor cells that are clear and arranged within the alveolar structure. The main indicator for the diagnosis of rhabdomyosarcoma is the identification of rhabdomyoblasts, which can be spindled/elongated or polygonal. E. Image depicting positive cytoplasmic immunostaining of tissue from Patient 10 for sarcoma-actin. F. Image of tissue from Patient 6 showing positive immunostaining for MyoD1 within nuclei. G. Image of tissue from Patient 12 showing positive immunostaining for myogenin within nuclei. H. Image of tissue from Patient 5 showing positive immunostaining for CD99 at the plasma membrane. I. Patients 5, 6, 7, 8, and 10 were positive for the PAX3-FKHR fusion transcript (147 bp), while Patient 12 was positive for the PAX7-FKHR fusion transcript (147 bp), as determined by RT-PCR. The transcript breakpoints between PAX3 and FKHR were confirmed by automated sequencing of the RT-PCR products.

part of the tumor cell cytoplasm being eosinophilic (**Figure 2A**). The alveolar structure and fibrous tissue split the tumor cells in the interstitial space (**Figure 2B**). Some cases showed monocytoid lymphocyte-like tumor cells, and the cytoplasm was empty (**Figure 2C**). Another case had tumor cells that were clear and arranged in the alveolar structure. The main clue for the diagnosis of rhabdomyosarcoma is the identification of rhabdomyoblasts, which can be spindled/elongated or polygonal (**Figure 2D**). The two cases of RCMLS examined in this study had solid, light gray-red tumors nodules, and were fish-shaped with jelly-like mucus (**Figure 3A**). The transitional area between the myxoid and small round tumor cells consisted of numerous undifferentiated tumor cells in addition to scattered univacuolar lipoblasts (**Figure 3B**). An alveolar structure and a prominent plexiform capillary pattern were observed, with some cells showing vacuolated cytoplasm, and a small number of the tumor cells showed

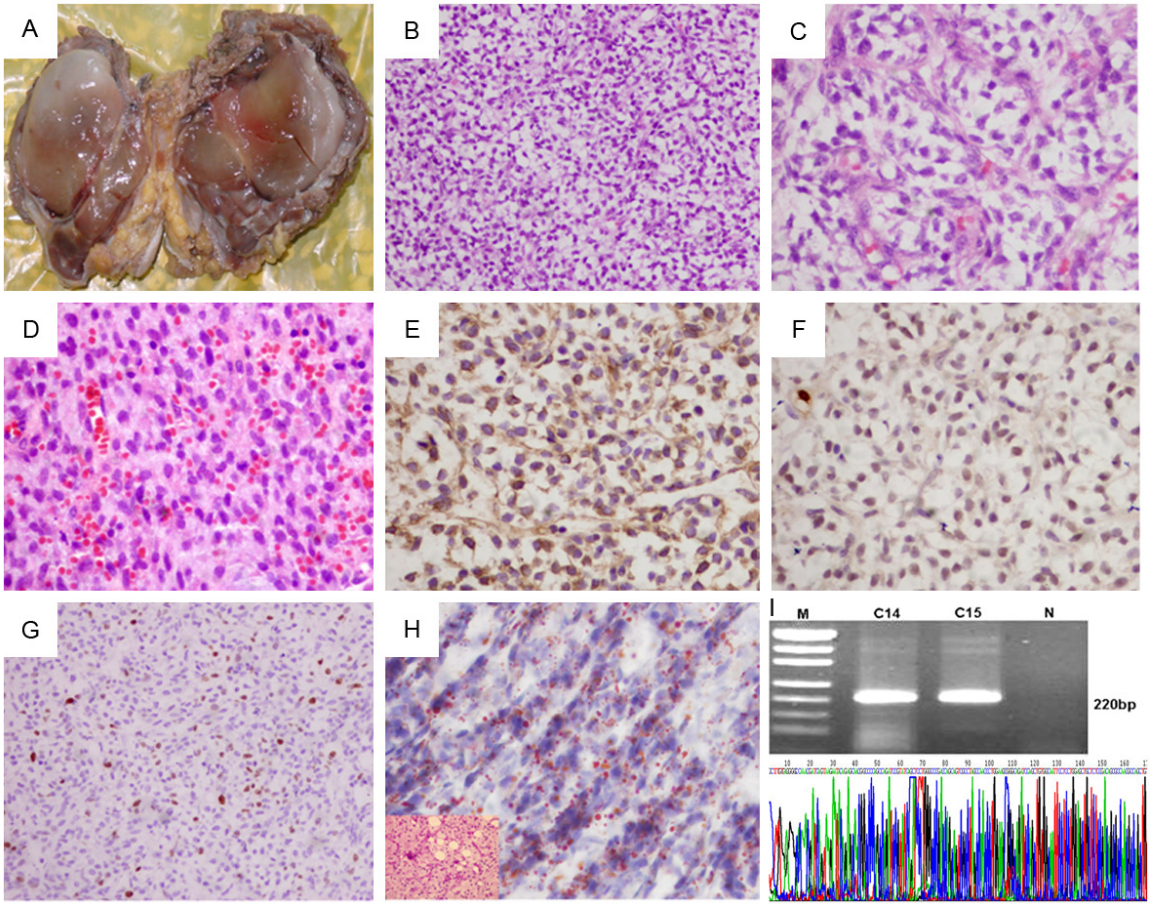

Figure 3. Histological, immunohistochemical, and reverse transcriptase-polymerase chain reaction (RT-PCR) analyses of round cell myxoid liposarcoma (RCMLS) tissues. Images of (A) a solid light gray red nodular tumor with mucus secretion and (B) the transitional area between myxoid and small round tumor cells consisting of numerous undifferentiated tumor cells in addition to scattered univacuolar lipoblasts. The main indicator for the diagnosis of RCMLS is the identification of atypical lipoblasts in focal area. (C) Image depicting the alveolar structure and a prominent plexiform capillary pattern of RCMLS tissues; certain cells exhibited vacuolated cytoplasm, while small numbers of tumor cells appeared ribbon-shaped and rhabdomyoblasts-like. (D) Tissue from Patient 14 showing diffuse distribution of small round tumor cells; the vascular pattern is obscured by the cellular proliferation. (E and F) Images of tissues from Patients 13 and 14 showing positive immunostaining for (E) vimentin and (F) S-100 within the cytoplasm and nuclei, respectively. (G) Low levels of Ki-67 staining in the tissues from Patient 14 indicate low levels of cell proliferation. (H) Images depicting the presence of orange droplets in the tissue from Patient 13, as determined by Oil Red O fat special staining, and of PAS-positive staining in the tissue from Patient 14. (I) Patients 13 and 14 were positive for the TLS-CHOP fusion transcript (220 bp), as determined by RT-PCR analysis and confirmed by automated sequencing of the RT-PCR products.

a ribbon-shaped rhabdomyoblast-like morphology (**Figure 3C**). In some cases, the small, round tumor cells were diffusely distributed, and the vascular pattern was obscured by cellular proliferation. The main clue for the diagnosis of RCMLS is the identification of atypical lipoblasts in the focal area (**Figure 3D**). Additionally, in some areas, the tumor cells were mucus fibrosarcoma-like. Lastly, the biopsy specimens from the four PDSS patients examined contained round or short shuttle-like tumor cells that were very small (**Figure 4E**). Most of the tumor cells displayed poor differentiation, with a scarce, irregular, clear (**Figure 4A**), and eosinophilic cytoplasm (**Figure 4E**), hyperchromatic round nuclei, and conspicuous nucleoli (**Figure 4D**). These tumors sometimes showed a hemangiopericytoma (**Figure 4C**), alveolar (**Figure 4B**) or Ewing-PNET-like round cell pattern (**Figure 4D**), or lack of biphasic differentiation characteristics.

IHC

IHC was employed to detect protein markers in cells of epithelial, mesenchymal, lymphoma, or

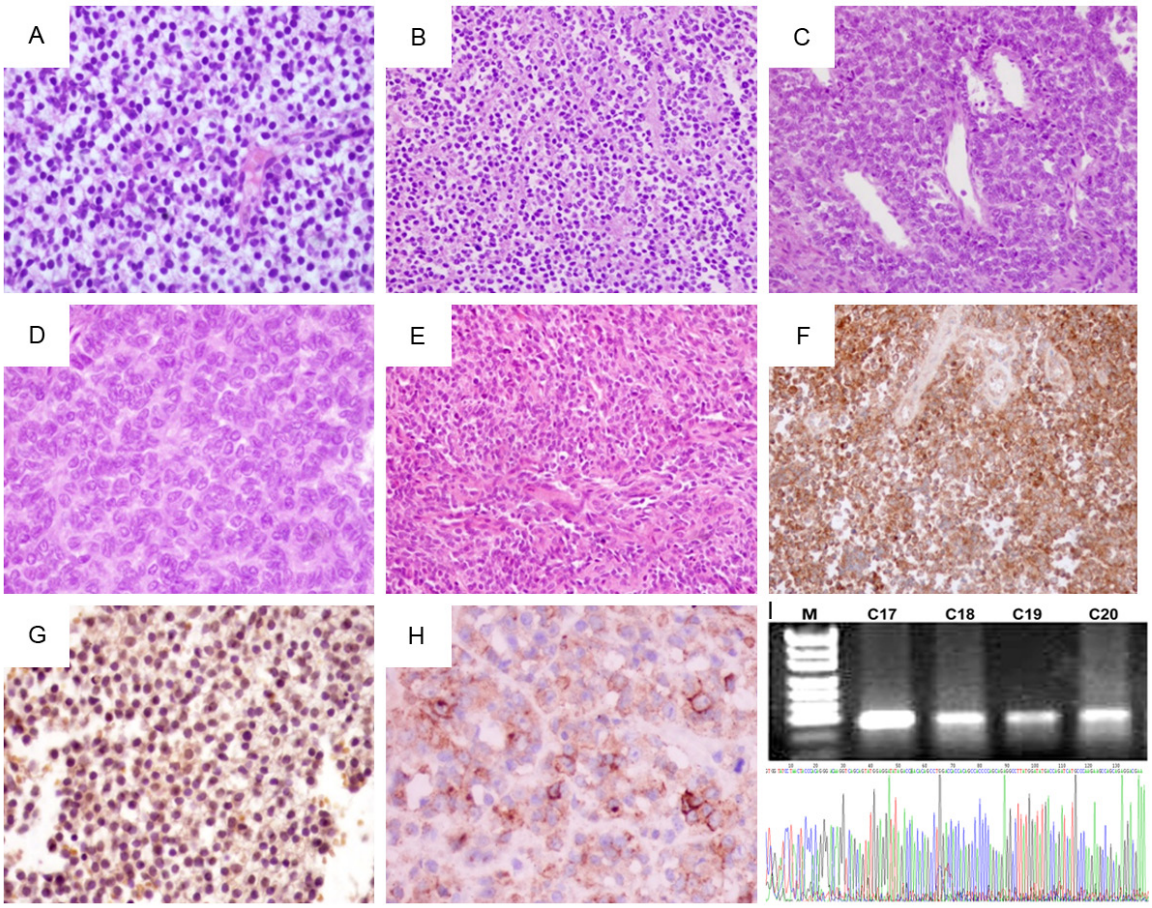

Figure 4. Histological, immunohistochemical, and reverse transcriptase-polymerase chain reaction (RT-PCR) analyses of poorly differentiated synovial sarcoma (PDSS) tissues. (A) Images of tissues from patients displaying primitive, undifferentiated small round or oval mesenchymal cells with clear cytoplasm and dense nuclei. (B) Image of tissue from Patient 18 showing division of tumor cells by an alveolar structure and fibrous tissue. (C) Image depicting the hemangiopericytoma-like pattern of PDSS. (D) Image depicting the Ewing-PNET-like round cell pattern observed in PDSS tissues. (E) Image of short-spindle cells observed in several patients. (F-H) Images depicting positive immunostaining of (F) CD99; (G) keratin; and (H) epithelial membrane antigen (EMA). (I) PDSS tissues were positive for the SYT-SSX fusion transcript (174 bp), as determined by RT-PCR analysis and confirmed by automated sequencing of the RT-PCR products.

neuroendocrine origin. The criteria for a positive cell were: positive vimentin, desmin, sarcomeric actin, epithelial membrane antigen (EMA), CK, LCA, NSE, and S-100 staining within the cytoplasm; positive CD99 staining at the cell membrane; and positive myogenin and MyoD1 staining in the nucleus. The results are summarized in **Table 3**. Positive CD99 immunostaining was observed in all five PNET samples. The staining intensity was strong in four and intermediate in one case. Positive nuclear immunostaining for FLI1 (**Figure 1G**) was observed in the five cases of PNET, and RT-PCR revealed evidence of the presence of *EWS-FLI1* fusion transcripts. Immunostaining for S-100 (**Figure 1F**) was positive in the nuclei in three cases. One case showed dramatic staining of desmin (**Figure 1H**), which led to confusion in diagnosis. A variable degree of cytoplasmic staining for desmin was observed in the seven ARMS (**Table 3**) tissues, which also exhibited strong or intermediate MyoD1 (**Figure 2G**) and myogenin (**Figure 2F**) immunoreactivity in tumor cells. Some ARMS and PDSS samples also showed CD99 (**Figures 2H**, **4F**) expression. The two RCMLS tissues were both vimentin- (**Figure 3E**) and S-100-positive (**Figure 3F**), but negative for the other proteins. The RCMLS tissues were also positive for Oil Red O fat-specific staining (**Figure 3H**) and intracellular glycogen, diastase-

Table 3. The results of 20 cases for IHC staining and fusion gene detecting

Case	CK	VIM	NSE	Sar-actin	CD99	Myogenin	MyoD1	DES	LCA	S-100	CD34	Fli-1	Other diagnostic markers	Fusion gene	Final dignosis
C1	-	+	+	-	+	-	-	+	-	-	No	+		EWS-FLI1	PNET
C2	-	-	+	+	+	-	-	-	-	+/-	-	+		EWS-FLI1	PNET
C3	-	+	+	+	+	-	-	-	-	+	-	+		EWS-FLI1	PNET
C4	-	+	+/-	-	+	-	-	-	-	+/-	-	+		EWS-FLI1	PNET
C5	-	+	+	-	+	-	-	-	-	-	-	-		PAX3-FKHR	ARMS
C6	-	-	+	+	+	+	+	+	-	+	-	-		PAX3-FKHR	ARMS
C7	-	+	+	+	+	-	+	+	-	-	No	-		PAX3-FKHR	ARMS
C8	-	+	+	+	+	+/-	+/-	+	-	-	No	+	HMB45$^{\Delta}$	PAX3-FKHR	ARMS
C9	-	+	+	-	-	+	-	+	-	-	-	-	SMA$^{\Delta}$, calponin$^{\Delta}$	Negative	ERMS
C10	-	+	-	+	+/-	+	+	-	-	-	No	-		PAX3-FKHR	ARMS
C11	-	+	+	No	+	No	-	-	-	No	-	+		EWS-FLI-1	PNET
C12	-	+	-	+	-	+	+	+	-	-	-	-		PAX7-FKHR	ARMS
C13	-	+	-	-	-	-	-	-	-	+	-	-		TLS-CHOP	MLS
C14	-	+	-	-	-	-	-	-	-	+	-	-	Calponin$^{\Delta}$, SMA$^{\Delta}$, CD68$^{\Delta}$	TLS-CHOP	MLS
C15	-	+	-	No	+	-	-	-	No	-	-	+	CD56$^{\blacktriangle}$, Bcl-2$^{\blacktriangle}$, WT-1$^{\blacktriangle}$; CK5/6$^{\Delta}$, CgA$^{\Delta}$, Syn$^{\Delta}$, EMA$^{\Delta}$, CAM5.2$^{\Delta}$, CD10$^{\Delta}$	EWS-FLI-1	PNET
C16	-	+	Focal+	-	+	-	-	-	Focal+	-	-	+	CD138$^{\blacktriangle}$; CD3$^{\Delta}$, TdT$^{\Delta}$, CD5$^{\Delta}$, CD7$^{\Delta}$, PAX-5$^{\Delta}$, CD21$^{\Delta}$, CD30$^{\Delta}$, CD15$^{\Delta}$	EWS-FLI-1	PNET
C17	-	+	-	-	+	-	-	-	-	+/-	-	-	Bcl-2$^{\Delta}$	SYT-SSX	PDSS
C18	Focal+	+	-	-	+	-	-	-	-	-	-	-	CD20$^{\Delta}$, CD3$^{\Delta}$	SYT-SSX	PDSS
C19	-	+	-	-	+	-	-	-	-	+/-	-	-		SYT-SSX	PDSS
C20	+	+	-	-	-	-	-	-	-	-	No	Focal+		SYT-SSX	PDSS

$^{\blacktriangle}$Positive; $^{\Delta}$Negative.

sensitive, and PAS-positive (**Figure 3H**) staining. Of the four PDSS cases, two were negative for AE1 and EMA, and did not show biphasic differentiation characteristics, whereas the other two cases showed positive cytokeratin (**Figure 4G**) and EMA (**Figure 4H**) staining at epithelial regions.

Nested mRT-PCR

We developed an assay that combined nested mRT-PCR and automated sequencing techniques. Four types of primers were designed for mRT-PCR amplification: chimeric primers and nested primers. Using this technique, we screened the 20 SCRSs tissues for the following fusion genes: *PAX3-FKHR* in ARMS, *TLS-CHOP* in RCMLS, *SYT-SSX* in PDSS, and *EWS-FLI1* in PNET. All seven of the PNET tissues harbored the *EWS-FLI1* fusion gene (**Figure 1I**). Meanwhile, of the seven ARMS tissues, five had the *PAX3-FKHR* fusion gene (**Figure 2I**), one harbored the *PAX7-FKHR* fusion gene (**Figure 2G**), and the last was fusion gene-negative. Lastly, both of the RCMLS cases harbored the *TLS-CHOP* fusion gene (**Figure 3I**), and each of the four PDSS tissues expressed the *SYT-SSX* fusion (**Figure 4I**). The identity of each of the amplified RT-PCR products was confirmed by automated sequencing.

Discussion

The advantages of RT-PCR for detection of fusion genes in soft tissue SRCSs patients have been described previously [10, 14, 15]. However, for some clinically difficult cases, carrying out multiple reactions for detection of distinct markers is impractical, time consuming, and costly. As such, the implementation of mRT-PCR, which enables the detection of multiple markers within a single reaction, could be advantageous. However, while mRT-PCR comprises an effective method for testing peripheral blood samples [16], it is more challenging to simultaneously detect multiple fusion genes in FFPE samples via this approach. The aim of the present study was therefore to develop an mRT-PCR method, based on detection of the PAX3-FKHR, EWS-FLI1, SYT-SSX, and TLS-CHOP fusion genes, which would enable clinical pathologist to rapidly and accurately diagnose complicated SRCSs patients.

Soft tissue SRCSs represent four of the most aggressive solid cancers arising from tissues of mesenchymal origin, and accurate diagnosis is critical to the clinical management of these patients [17]. Unlike the carcinomas that account for the majority of adult tumors or the embryonic tumors of infancy, most SRCSs can occur in all age groups, and are fairly common among patients aged between 15 and 29 years [defined here as adolescents and young adults (AYA)]. Soft tissue sarcomas constitute less than 1% of all adult malignancies, and the highest incidences of these cancers occur in the fifth decade of life [18]. Several lines of evidence suggest that sarcomas can be divided into two major genetic groups: those with non-specific genetic alterations and complex unbalanced karyotypes, and those with specific genetic alterations that typically exhibit simple karyotypes, such as reciprocal chromosomal translocations (e.g., TLS-CHOP in MLS/RCL; PAX-FKHR in ARMS; EWS-FLI1 in PNET; SYT-SSX in SS, etc.) [6, 19]. Most primitive soft tissue SRCSs belong to the later group, and the histogenesis of these SRCSs is uncertain. Thus, diagnosis and therapy remain a challenge for surgical pathologists [20], and molecular analyses are often necessary for pathological diagnosis of unusual histotypes.

For all cancers, accurate diagnosis is critical for disease management and patient outcomes. Notably, many SRCS patients receive disparate diagnostic opinions. As such, the misdiagnosis rate among these patients is very high. Usually, immunohistochemistry, electron microscopy, and specific staining provide useful information for clinical diagnoses. For example, CD99 staining is an indicator of EN/PNET [9], while Desmin, MyoD1, and Mygenin are specific markers for RMS [21].

However, most tumors lack specific antigens. Moreover, one type of tumor can express multiple antigens, while a given antigen can be expressed by multiple tumor types. Thus, aberrant antigen expression can make diagnosis difficult, particularly for certain SRCSs. As a result, RT-PCR and FISH molecular genetic analyses have already become an integral part of the work-up for SRCSs that demonstrate characteristic translocations, and have enhanced the rates of accurate diagnosis of these cancers [6].

In a previous study, Naito et al. [22] screened 75 soft tissue sarcomas (STS) patients for various fusion transcripts by RT-PCR and conclud-

ed that this method comprised a useful tool for confirmation of STS diagnoses in adults in situations where diagnosis is difficult, as well as in retrospective studies. Meanwhile, mRT-PCR has recently been used as a screening tool for detection of genetic rearrangements, for in vitro toxicology screening [23], and for validation of gene sets obtained from global screens [24]. Moreover, Chen et al. [17] recently used mRT-PCR for blind testing of 96 small round blue cell tumors. Thus, this method offers a powerful diagnostic tool for achieving rapid diagnosis using a minimal amount of tissue. In this study, we therefore developed a rapid and reliable diagnostic mRT-PCR assay to distinguish SRCSs according to their diagnostic categories, and subsequently verified the results using a one-step RT-PCR approach. Our method was effective, as blind testing of the 20 samples included in the study demonstrated that all samples contained the small round cells indicative of mesenchymal tumors. This study is efficiently equivalent to an independent study because the target genes chosen were based on the results of our previous soft tissue sarcoma study [25], and the primers used were validated using an independent set of tumors, which we had not evaluated previously. To the best of our knowledge, myxoid/round cell liposarcomas can typically be diagnosed by morphological analysis alone. However, we included this cancer type in the current for identifying some difficult cases.

In conclusion, immunohistochemical evaluation is typically the first choice for diagnosing SRCSs, as it is convenient, efficient, and cost-effective [26, 27]. However, this method occasionally leads to diagnostic difficulties owing to the fact that certain immunohistochemical markers can be expressed in multiple tumor types. In such cases, this issue is resolved via molecular techniques. In this study, we improved on current diagnostic technology by developing an mRT-PCR assay that can discriminate between distinct soft tissue SRCS types by detecting fusion genes specific to these sarcomas. mRT-PCR is advantageous in that it is relatively simple, rapid, and cost-effective, compared to other diagnostic steps that are considered in difficult cases, including clinicoradiologic correlation, molecular genetics, and cytogenetic methods.

Acknowledgements

This work was supported by grants from the National Natural Science Foundation of China (Nos. 81560053), the Outstanding Youth Science and Technology Talent Cultivation Plan of Shihezi University (Nos. 2015ZRKXJQ07 and 2013ZRKXJQ05), the Corps Doctor Foundation (No. 2014BB018), and the Research Project of High Level Talents of Shihezi University (No. RCZX201549).

Disclosure of conflict of interest

None.

Authors' contribution

YQ and JLZ carried out the molecular genetic studies and drafted the manuscript. JMH and WJ participated in the follow-up investigation. JFJ and JZ participated in the design of the study and performed the histological and immunohistochemical analyses. NW and HZ performed fusion gene detection. LJP, FL and YQ conceived of the study, participated in its design and coordination, and helped to draft the manuscript. All authors have read and approved the final manuscript.

Address correspondence to: Dr. Lijuan Pang, Department of Pathology and The Laboratory of Xinjiang Endemic and Ethnic Diseases, School of Medicine, Shihezi University, Shihezi, Xinjiang, China; Dr. Feng Li, Department of Pathology, Beijing Chaoyang Hospital, Capital Medical University, Beijing, China. Tel: 86-993-2057125; Fax: 86-993-2057136; E-mail: ocean123456@163.com (LJP); E-mail: lifeng7855@126.com (FL)

References

[1] Mertens F, Tayebwa J. Evolving techniques for gene fusion detection in soft tissue tumours. Histopathology 2014; 64: 151-162.

[2] Taylor BS, Barretina J, Maki RG, Antonescu CR, Singer S, Ladanyi M. Advances in sarcoma genomics and new therapeutic targets. Nat Rev Cancer 2011; 11: 541-557.

[3] Chang CC, Shidham VB. Molecular genetics of pediatric soft tissue tumors: clinical application. J Mol Diagn 2003; 5: 143-154.

[4] Pfeifer JD, Hill DA, O'Sullivan MJ, Dehner LP. Diagnostic gold standard for soft tissue tumours: morphology or molecular genetics? Histopathology 2000; 37: 485-500.

[5] Sandberg AA, Bridge JA. Updates on the cytogenetics and molecular genetics of bone and soft tissue tumors. gastrointestinal stromal tumors. Cancer Genet Cytogenet 2002; 135: 1-22.
[6] Antonescu CR. The role of genetic testing in soft tissue sarcoma. Histopathology 2006; 48: 13-21.
[7] Elnifro EM, Ashshi AM, Cooper RJ, Klapper PE. Multiplex PCR: optimization and application in diagnostic virology. Clin Microbiol Rev 2000; 13: 559-570.
[8] Peter M, Gilbert E, Delattre O. A multiplex real-time pcr assay for the detection of gene fusions observed in solid tumors. Lab Invest 2001; 81: 905-912.
[9] Folpe AL, Hill CE, Parham DM, O'Shea PA, Weiss SW. Immunohistochemical detection of FLI-1 protein expression: a study of 132 round cell tumors with emphasis on CD99-positive mimics of Ewing's sarcoma/primitive neuroectodermal tumor. Am J Surg Pathol 2000; 24: 1657-1662.
[10] Chang B, Pang LJ, Qi Y, Liu CX, Cao Y, Li HA, Hu WH, Jiang JF, Zhang WJ, Li F. PAX--FKHR fusion genes and AChR-gamma in Chinese patients with rhabdomyosarcoma: diagnosis using formalin-fixed archival tissues. Int J Surg Pathol 2009; 17: 6-15.
[11] Cha RS, Thilly WG. Specificity, efficiency, and fidelity of PCR. PCR Methods Appl 1993; 3: S18-29.
[12] Henegariu O, Heerema NA, Dlouhy SR, Vance GH, Vogt PH. Multiplex PCR: critical parameters and step-by-step protocol. Biotechniques 1997; 23: 504-511.
[13] Markoulatos P, Siafakas N, Moncany M. Multiplex polymerase chain reaction: a practical approach. J Clin Lab Anal 2002; 16: 47-51.
[14] Sugita S, Arai Y, Tonooka A, Hama N, Totoki Y, Fujii T, Aoyama T, Asanuma H, Tsukahara T, Kaya M, Shibata T, Hasegawa T. A novel CIC-FOXO4 gene fusion in undifferentiated small round cell sarcoma: a genetically distinct variant of Ewing-like sarcoma. Am J Surg Pathol 2014; 38: 1571-1576.
[15] Ren T, Lu Q, Guo W, Lou Z, Peng X, Jiao G, Sun Y. The clinical implication of SS18-SSX fusion gene in synovial sarcoma. Br J Cancer 2013; 109: 2279-2285.
[16] Taback B, Chan AD, Kuo CT, Bostick PJ, Wang HJ, Giuliano AE, Hoon DS. Detection of occult metastatic breast cancer cells in blood by a multimolecular marker assay: correlation with clinical stage of disease. Cancer Res 2001; 61: 8845-8850.
[17] Chen QR, Vansant G, Oades K, Pickering M, Wei JS, Song YK, Monforte J, Khan J. Diagnosis of the small round blue cell tumors using multiplex polymerase chain reaction. J Mol Diagn 2007; 9: 80-88.
[18] Kasper B, Ouali M, van Glabbeke M, Blay JY, Bramwell VH, Woll PJ, Hohenberger P, Schoffski P. Prognostic factors in adolescents and young adults (AYA) with high risk soft tissue sarcoma (STS) treated by adjuvant chemotherapy: a study based on pooled European Organisation for Research and Treatment of Cancer (EORTC) clinical trials 62771 and 62931. Eur J Cancer 2013; 49: 449-456.
[19] Lazar A, Abruzzo LV, Pollock RE, Lee S, Czerniak B. Molecular diagnosis of sarcomas: chromosomal translocations in sarcomas. Arch Pathol Lab Med 2006; 130: 1199-1207.
[20] Kerouanton A, Jimenez I, Cellier C, Laurence V, Helfre S, Pannier S, Mary P, Freneaux P, Orbach D. Synovial sarcoma in children and adolescents. J Pediatr Hematol Oncol 2014; 36: 257-262.
[21] Sebire NJ, Malone M. Myogenin and MyoD1 expression in paediatric rhabdomyosarcomas. J Clin Pathol 2003; 56: 412-416.
[22] Naito N, Kawai A, Ouchida M, Dan'ura T, Morimoto Y, Ozaki T, Shimizu K, Inoue H. A reverse transcriptase-polymerase chain reaction assay in the diagnosis of soft tissue sarcomas. Cancer 2000; 89: 1992-1998.
[23] Pauly A, Meloni M, Brignole-Baudouin F, Warnet JM, Baudouin C. Multiple endpoint analysis of the 3D-reconstituted corneal epithelium after treatment with benzalkonium chloride: early detection of toxic damage. Invest Ophthalmol Vis Sci 2009; 50: 1644-1652.
[24] Tan CK, Carey AJ, Cui X, Webb RI, Ipe D, Crowley M, Cripps AW, Benjamin WH Jr, Ulett KB, Schembri MA, Ulett GC. Genome-wide mapping of cystitis due to Streptococcus agalactiae and Escherichia coli in mice identifies a unique bladder transcriptome that signifies pathogen-specific antimicrobial defense against urinary tract infection. Infect Immun 2012; 80: 3145-3160.
[25] Qi Y, Chang B, Pang LJ, Liu CX, Hu WH, Li HA, Jiang JF, Gao JF, Wei JY, Li F. [Multiplex RT-PCR assay for detecting fusion genes of soft tissue small round cell tumors using paraffin-embedded and formalin-fixed tissue]. Zhonghua Bing Li Xue Za Zhi 2006; 35: 634-636.
[26] Miettinen M. Immunohistochemistry of soft tissue tumours - review with emphasis on 10 markers. Histopathology 2014; 64: 101-118.
[27] Fisher C. Immunohistochemistry in diagnosis of soft tissue tumours. Histopathology 2011; 58: 1001-1012.